Medical Engineering & Physics 34 (2012) 211–218

Contents lists available at ScienceDirect

Medical Engineering & Physics

journal homepage: www.elsevier.com/locate/medengphy

Experimental investigation of the flow of a blood analogue fluid in a replica of a bifurcated small artery

A.D. Anastasiou [a], A.S. Spyrogianni [a], K.C. Koskinas [b], G.D. Giannoglou [b], S.V. Paras [a,*]

[a] Laboratory of Chemical Process and Plant Design, Department of Chemical Engineering, Aristotle University of Thessaloniki, Thessaloniki, Greece
[b] Cardiovascular Engineering and Atherosclerosis Laboratory, 1st Cardiology Department, AHEPA University Hospital, Medical School, Aristotle University of Thessaloniki, Thessaloniki, Greece

ARTICLE INFO

Article history:
Received 1 February 2011
Received in revised form 31 May 2011
Accepted 13 July 2011

Keywords:
Non-Newtonian fluid
μ-PIV
Small arteries
Wall shear stress
Atherosclerosis

ABSTRACT

The scope of this work is to study the pulsatile flow of a blood mimicking fluid in a micro channel that simulates a bifurcated small artery, in which the *Fahraeus–Lindqvist* effect is insignificant. An aqueous glycerol solution with small amounts of xanthan gum was used for simulating viscoelastic properties of blood and *in vivo* flow conditions were reproduced. Local flow velocities were measured using micro Particle Image Velocimetry (μ-*PIV*). From the measured velocity distributions, the wall shear stress (*WSS*) and its variation during a pulse were estimated. The Reynolds numbers employed are relatively low, i.e. similar to those prevailing during blood flow in small arteries. Experiments both with a Newtonian and a non-Newtonian fluid (having asymptotic viscosity equal to the viscosity of the Newtonian one) proved that the common assumption that blood behaves as a Newtonian fluid is not valid for blood flow in small arteries. It was also shown that the outer wall of the bifurcation, which is exposed to a lower *WSS*, is more predisposed to atherosclerotic plaque formation. Moreover, this region in small vessels is shorter than the one in large arteries, as the developed secondary flow decays faster. Finally, the *WSS* values in small arteries were found to be lower than those in large ones.

1. Introduction

The study of blood velocity distribution in blood vessels can be proved very important for biomedical engineering with significant clinical implications. Moreover, blood flow modeling is helpful in therapy strategy and the design of surgical repairements and implantable medical devices [1]. In recent papers [2,3] it is reported that local hemodynamic forces affect the incipient formation as well as the progression rate of the atherosclerotic plaque, that occurs mainly in regions of curvature, bifurcation, and branching of the vessels. Low *WSS* values promote the formation of atherosclerotic plaque [2], while higher shear stresses exert atheroprotective function by promoting the release of the potent vasodilators nitric oxide and prostacyclin [4].

In Fig. 1 [2] the effect of *WSS* on the formation and progression of atherosclerotic plaque is described. Low blood velocity, i.e. low *WSS* (Fig. 1a), leads to an increased concentration of particles responsible for atherosclerosis, i.e. low density lipoprotein, at the lumen surface, while at the same time increases the permeability of the endothelial layer to circulating lipoproteins. These phenomena enhance the subendothelial migration and accumulation of blood atherogenic particles, promoting lesion formation. The progression of the lesion (Fig. 1b) leads to an artery stenosis, which acts as a forward and backward-facing step. It is known [5] that the minimum wall shear stress on a stepped wall occurs behind the backward-facing step, in the neighborhood of the reattaching flow region. This leads to progression of the plaque downstream of the lesion (Fig. 1c). Considering all the aforementioned phenomena, atherosclerosis is clearly affected by biomechanical factors.

Atherosclerosis typically affects large- and medium-sized arteries. However, evidence from the literature suggests that the coronary microcirculation, consisting of arteries with a diameter around to 600 μm, critically influence coronary blood flow and myocardial perfusion [6]. Damages in small vessels, which could be related to atherosclerosis, have been also reported by Kuo et al. [7], who extensively described the consequences of atherosclerosis to coronary microcirculation as well as Bund et al. [8], who reported that subcutaneous small arteries from patients with Syndrome *X* are characterized by increased thickness. Histologic and epidemiologic studies show consistent differences in the occurrence and progression rates of atherosclerotic lesions in large and small vessels. This can be partly explained by the different biological properties of the endothelium a fact that is supported by evidence given by various investigators (as summarized in a review paper by Aboyans et al. [9]). In distal arteries, apart

* Corresponding author at: University Box 455, Thessaloniki GR 54124, Greece. Tel.: +30 2310 996174; fax: +30 2310 996209.
E-mail address: paras@auth.gr (S.V. Paras).

1350-4533/$ – see front matter © 2011 IPEM. Published by Elsevier Ltd. All rights reserved.
doi:10.1016/j.medengphy.2011.07.012

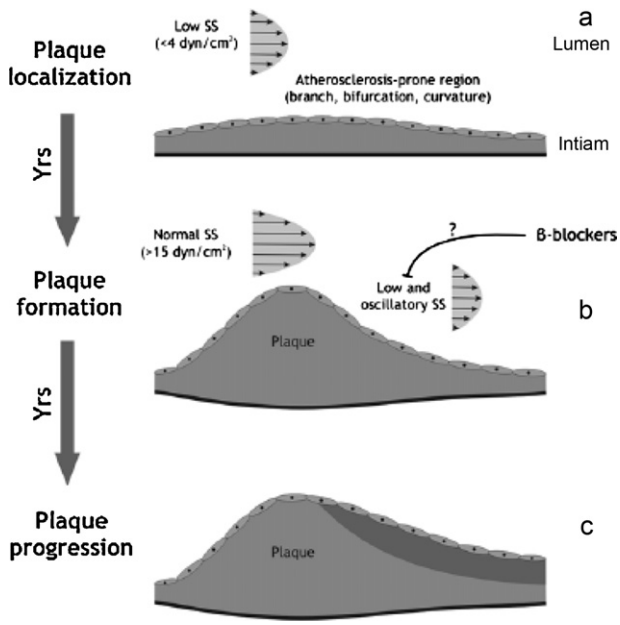

Fig. 1. Plaque formation and progression due to low *WSS* [2].

Table 1
Geometrical characteristics and flow conditions for human arteries [10].

	Radius (cm)	*Re* number	Womersley number (a)
Proximal aorta	1.500	1500	21.70
Femoral artery	0.270	180	3.90
Left coronary artery	0.425	270	6.14
Left anterior descending coronary artery	0.170	80	2.40
Right coronary	0.097	233	1.82
Terminal arteries	0.050	17	0.72

from the diameter, the flow rate differs considerably from that in large vessels, and thus *Reynolds* numbers are expected to be about ten times lower than those in proximal ones (Table 1) [10]. It is also known that diabetes, i.e. a high blood glucose concentration which affects the asymptotic viscosity, is associated with small vessel disease [9]. However, the parameters affecting this association have not being thoroughly investigated. Taking all these into account the independent investigation of hemodynamic behavior can be regarded as an essential initial step towards understanding and interpreting atherosclerosis in small distal vessels.

Numerous works have been published on blood flow or on atherosclerosis and *WSS* in large and medium sized arteries, especially the coronary arteries (e.g. [11–16]). On the contrary, flow in small vessels has not been sufficiently studied. As it is noticed by Aboyans et al. [9], even the term "*small artery*" is not well defined in the research community. The majority of the works that study the hemodynamic conditions in small blood vessels refer to lumen diameters up to 100 μm (e.g. [17–22]). In such small vessels, though, red blood cells drift to the central axis of the vessel and a cell-free layer, called a plasma layer, is formed along the vascular wall. As a result the apparent blood viscosity declines substantially with decreasing diameter, a behavior known as the *Fahraeus–Lindqvist* effect. This effect is significant for blood vessels with diameter smaller than 300 μm [23]. Additionally, in the *in vitro* aforementioned studies [17–19] the working fluids were dilute aqueous solutions of red blood cells, corresponding to low haematocrit (*Ht*) levels, i.e. up to 20%. Consequently, the research of blood flow in small arteries where the *Fahraeus–Lindqvist* effect can be considered negligible (i.e. blood is regarded as a non-Newtonian homogenous fluid) for physiological *Ht* levels seems to be the missing part from the vascular network investigation.

The present work focuses on the *in vitro* investigation of blood flow, under physiological conditions, in a replica of a bifurcated small artery with hydraulic diameter 600 μm. Namely, the flow of blood with $Ht \sim 45\%$ is studied by employing a blood analogue whose local velocity distributions are measured. The *WSS* values are also estimated in the vicinity of the bifurcation.

2. *In vivo* flow conditions

Blood is a multiphase mixture of plasma, a Newtonian fluid, and three main cell types, namely red blood cells, platelets and leukocytes. Under low shear rate normal red cells form linear aggregates (rouleaux) which disrupt flow streamlines and greatly increase the apparent blood viscosity. By increasing the shear rate these aggregates are progressively deformed and consequently the apparent viscosity decreases to an asymptotic limit, which is equal to 3.5 mPa s for $Ht \sim 45\%$ [24]. Thus, blood is a non-Newtonian fluid with shear thinning behavior that relies on its chemical composition. Although many researchers regard blood as a Newtonian fluid, a rather reasonable assumption for the high shear rates existing in large arteries (e.g. [16,25,26]), Gijsen et al. [14] suggested that this may not be accurate enough as the viscoelastic properties affect blood flow dynamics. In this study, aiming to validate the above assumption for flow in small arteries, experiments are conducted employing both a non-Newtonian and a Newtonian blood analogue.

It is well known that *in vivo* blood flow varies during the two phases of the heart cycle. Specifically, the pressure and the volumetric flow rate of the blood vary with time over the period of heart contraction and relaxation and hence the diameter of the large arteries changes significantly during a pulse. It is also known [10] that the maximum pressure declines and the pulse width broadens with increasing distance from the heart. Thus in small arteries there is no significant change in lumen diameter and their walls could be regarded rigid.

3. Velocity measurement method

Since measuring blood velocity *in vivo* is difficult, most experiments reported in the literature have been conducted *in vitro*, using methods like *Laser Doppler Anemometry* [12,13] and *Ultrasonic Velocimetry* [27]. A relatively new method for velocity measurements in micro channels is μ-*PIV*, which is a non-intrusive technique for measuring two dimensional velocity fields. There are several works that use μ-*PIV* to study biological systems (e.g. [18,20,21]). For a μ-*PIV* measurement flow-tracing seeded particles are used whose choice is crucial for the validity of the measurements. They must be small enough to follow the fluid motion accurately and to avoid microchannel obstruction, while at the same time they must be large enough for being adequately imaged and for avoiding Brownian motion. A velocity measurement is based on at least two successive images of the particles, along a known and short time interval (Δt). After pre-processing, background removal and signal amplification, the acquired images are divided in sub-areas usually called "*interrogation areas*". The displacement (Δx) of a group of particles is calculated by cross-correlating the sub-area from the first image and the corresponding one from the second image. Finally, the velocity (U) can be calculated as the ratio of Δx over Δt. The most important limitation to the use of μ-*PIV* is that the vessel walls must be transparent, a fact that renders *in vivo* measurements in human vessels non feasible.

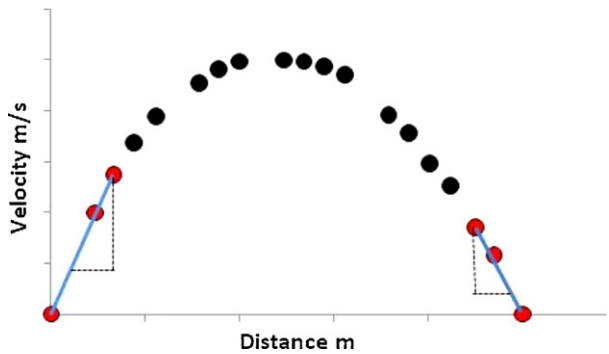

Fig. 2. Estimation of wall shear rate from velocity data.

4. Wall shear stress (WSS) estimation

The use of special electro-diffusion probes mounted in the channel wall allows direct measurements of *WSS* in the macro scale [28]. However, the same measurements in micro-channels or in channels with elastic walls are difficult to perform. In this case the *WSS* is usually estimated using methods based on curve fitting on the measured velocity data [29]. In the present work it is assumed that the velocity distribution near the wall is *linear*. Using two velocity measurements near the wall and the zero velocity on the wall as a third one, a straight line is drawn (Fig. 2), whose *slope* represents the shear rate near the wall ($\dot{\gamma}$). As the two measurements are close enough, the use of three points instead of two reduces the uncertainty of the estimation. Substituting the value of $\dot{\gamma}$ in the appropriate viscosity equation, which depends on the fluid employed, the *WSS* can be estimated with reasonable accuracy.

5. Experimental procedure and setup

Since, due to coagulation, conducting experiments with blood is a difficult task, blood mimicking fluids, i.e. fluids with similar rheological properties, were developed. Thus, with the intention of simulating the non-Newtonian behavior of human blood with Ht ~ 45% various aqueous solutions of glycerol and xanthan gum were prepared (Table 2). Xanthan gum is a polysaccharide that acts as rheology modifier and renders the fluid non-Newtonian. The viscosity of these solutions was measured with a cone plate rheometer (*AR-G2*, *TA Instruments*). In Fig. 3 the viscosities of the blood analogues were compared with the viscosity of blood as it is given by [30,31]. *Blood analogue 4*, which comprises 79.1% (v/v) distilled water, 20.9% (v/v) glycerol and 0.021% (w/v) xanthan gum, was found to be the most suitable for simulating viscoelastic properties of blood, for shear rates ranging from 1 to 1000 s^{-1} and it was the one used for the experiments. The shear stress vs. shear rate relationship for the blood analogue follows the model of *Herschel–Bulkley* (Eq. (1)) with standard error of fit 6.5%, and this is used for estimating the *WSS*, τ_y.

$$\tau_y = A + B\dot{\gamma}^C \quad (1)$$

where *A*: yield stress, 0.02160 (Pa); *B*: viscosity coefficient, 0.01345 (Pa $s^{1/c}$); *C*: rate index, 0.7812.

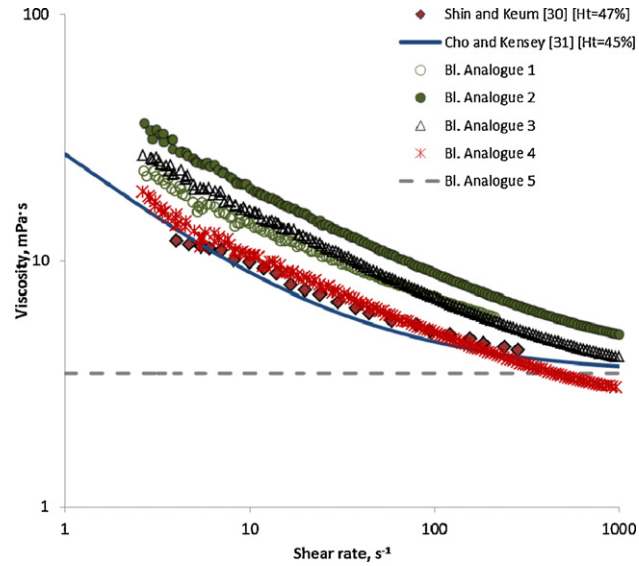

Fig. 3. Comparison of viscosity between real blood and the blood analogue fluids.

Blood analogue 5, which is used as a reference, is a Newtonian, aqueous solution of glycerol (32.6%, v/v), whose viscosity equals the asymptotic viscosity of blood (3.5 mPa s).

Aiming to mimic physiological flow conditions, pulsatile flow is generated in the parent channel using a syringe-pump (*Alladdin*, *Al-2000*). Assuming that flow rates in small arteries depend on the distance from the heart, two different pulses (with attenuated amplitude with respect to the initial one of the heart) were used (Fig. 4); the first of which corresponds to regions with relatively high flow rates (*case 1*: 140–340 ml/h), while the second to regions with relatively low flow rates (*case 2*: 20–60 ml/h). For both cases the pulse frequency is 1 Hz (i.e. 60 heart beats/min), while for these flow conditions the Reynolds number (*Re*) ranges from 9 to 21 (*case 1*) and from 1.1 to 3.5 (*case 2*). An important quantity to be taken into account in pulsatile flow is Womersley number, which is the ratio of transient inertia over viscous forces and is defined as $\alpha = R\sqrt{\omega\rho/\mu}$, where ω is the angular frequency, *R* the radius of the vessel, ρ the density and μ the dynamic viscosity. However for the present study Wormesley number retains a constant value (α = 0.42), because both the diameter of the micro channel and the frequency of the pulse are constant.

All experiments were conducted in a 600 μm hydraulic diameter channel (matching small artery dimensions) manufactured by laser ablation in a polymeric chip and sealed with the same material. The geometric characteristics of the test section are presented in Fig. 5. The velocity data were acquired from the middle plane of the bifurcation, i.e. 300 μm over the channel bottom at three stations along the conduit, namely upstream (*station 1*), at the entrance of (*station 2*) and one diameter downstream (*station 3*) of the bifurcation (Fig. 5). As the two daughter channels have the same diameter and the symmetry of the flow was checked, measurements were conducted only in one of the daughter channels of the bifurcation.

A backlight μ-*PIV* system was used to study the flow. The measuring section of the micro channel was illuminated by a micro

Table 2
Composition and properties of blood analogues.

Blood analogue	1	2	3	4	5
Glycerol (%, v/v)	29.90	29.90	25.30	20.90	32.60
Dist. water (%, v/v)	70.10	70.10	74.70	79.10	67.40
Xanth. gum (%, w/v)	0.027	0.032	0.032	0.021	–
Density (kg/m^3)	1076	1076	1064	1052	1083
Asymptotic viscosity (mPa s)	4.49	5.03	4.07	3.32	3.50

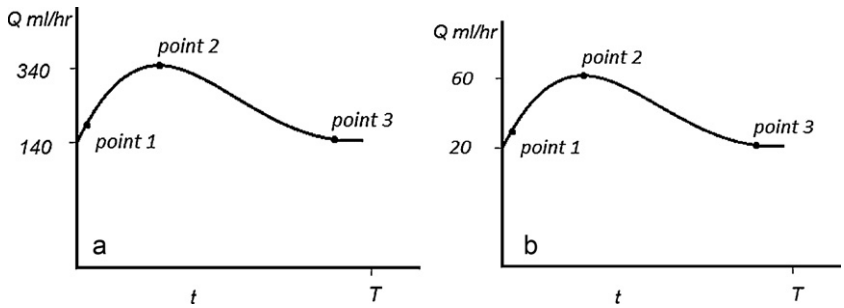

Fig. 4. Schematic of pulse employed for: (a) high flow rate and (b) low flow rate.

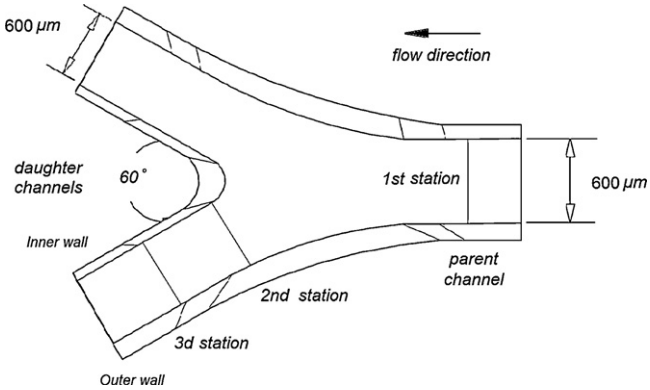

Fig. 5. Bifurcation geometry and the three positions of measurements.

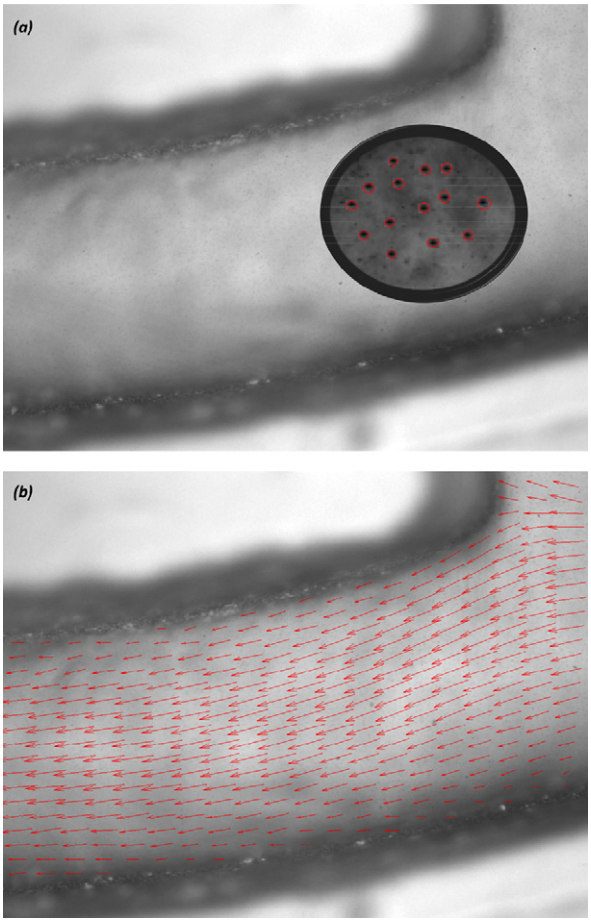

Fig. 6. Daughter channel of the bifurcation: (a) seeded particles; (b) velocity vectors from μ-*PIV* measurements.

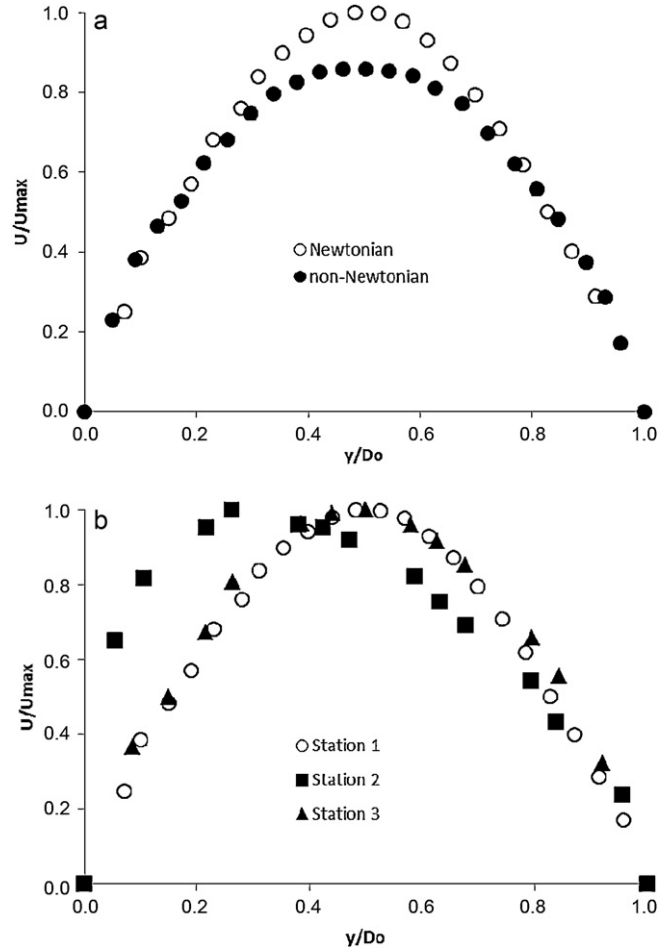

Fig. 7. Normalized velocity profiles with respect to their maximum value for steady flow conditions: (a) for the Newtonian and non-Newtonian fluids at *station 1* and (b) for the Newtonian fluid at *stations 1–3*.

strobe emitting at 532 nm. The flow was recorded using a high sense *CCD* camera, connected to a Nikon microscope. The flow was traced by adding polystyrene particles with mean diameter of 1 μm (Fig. 6a). In order to obtain magnified images a *10X* air immersion objective with *NA* = 0.30 was used and this corresponds to 37 μm depth of field. Velocity data acquired at a distance from the wall less than 50 μm would have been unreliable, because shadows interfere with the measurements in the vicinity of the wall. The time delay between frames lies in the range of 100–350 μs, while the sampling rate is 5 Hz. For every flow rate and station 200 images were acquired. Finally, the image processing and the velocity estimations were performed using *Flow Manager* Software (*DantecDynamics*).

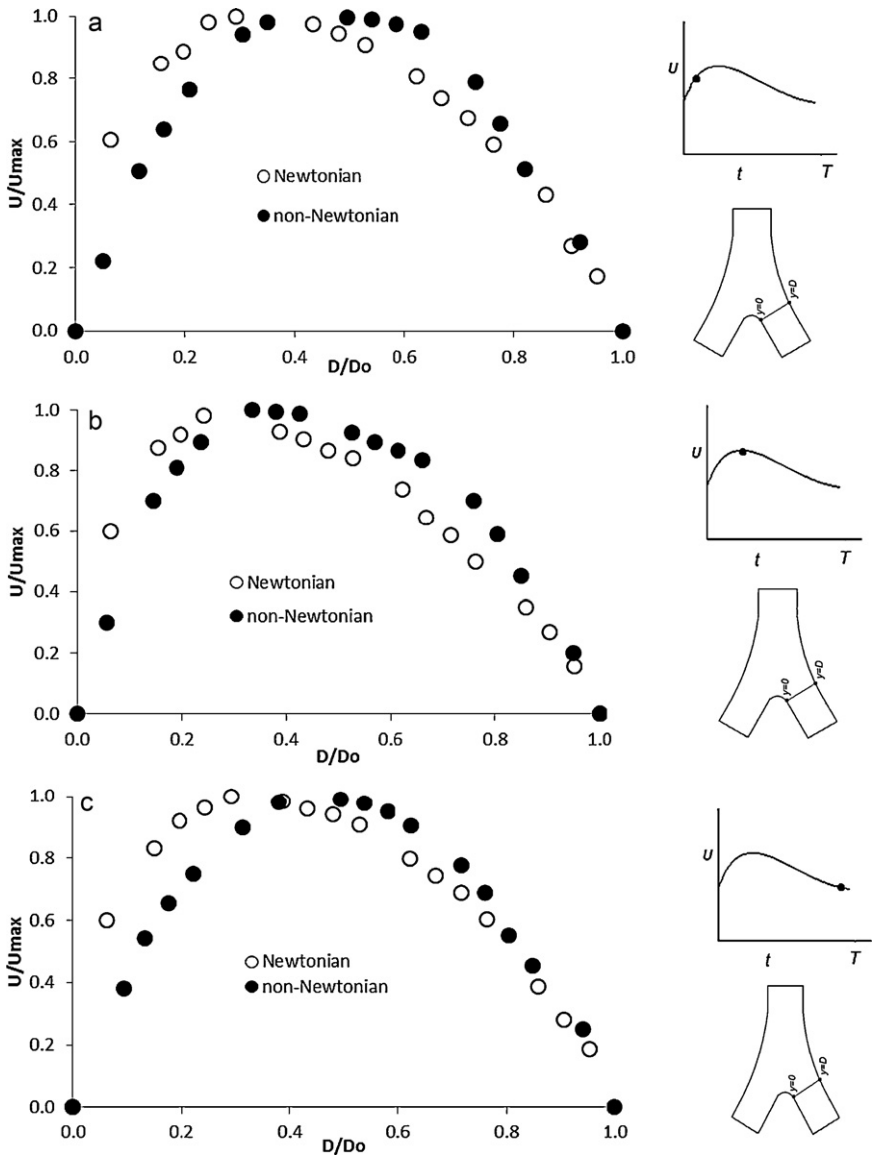

Fig. 8. Normalized velocity profiles with respect to their maximum value for Newtonian and non-Newtonian fluid at *station 2* for each instant of the pulse for *case 1* (*Re* = 9–21).

6. Results and discussion

Typical velocity profiles for various experimental conditions are presented in Fig. 7. In Fig. 7a the velocity data are normalized with respect to the maximum velocity of the Newtonian fluid, whereas in Figs. 7b, 8 and 9 the velocity data are normalized with respect to the maximum velocity of the corresponding fluid. In Fig. 7a the velocity distribution at *station 1* is presented for both the Newtonian and the non-Newtonian blood analogue for *steady* flow conditions and as expected the latter exhibits a flat velocity profile. In Fig. 7b the velocity profile for the Newtonian fluid is presented for *case 1* and for all three stations. It is observed that at *station 2* the position of the maximum axial velocity is shifted towards the inner channel wall. This is expected since it is known that transverse secondary flows are developed in curved conduits as a result of the interplay between centrifugal and viscous forces. Given that the driving centrifugal force depends quadratically, while the viscous force depends linearly on average velocity, secondary flows are strongly suppressed for low velocities. According to Paras [32], who conducted experiments that simulate flow in human airways, for *Re* < 30 the secondary flow decays before the first diameter downstream the junction. This is verified by observing Fig. 7b, where the velocity profile is parabolic at *station 1*, the maximum velocity is shifted after entering the bifurcation (*station 2*) and finally returns to the initial parabolic profile after a length of *one* diameter (*station 3*). On the contrary in *large* arteries secondary flow does not decay so fast. The length required for the velocity profile to return to the initial parabolic one depends on the *Re* and consequently is greater in these arteries (e.g. after 6 diameters for *Re* = 92.2 as reported by Chen et al. [33]).

Figs. 8 and 9 velocity measurements at the entrance of the daughter channel (*station 2*) for *both fluids* tested and at *three* typical instants of the pulse are compared. As shown in Fig. 8 (*case 1* and *Re* 9–21) the velocity distributions for the two fluids are different. More specifically, for the Newtonian fluid the maximum velocity is shifted from the centerline towards the inner wall of the channel during one pulse cycle. This displacement is not so intense in the case of non-Newtonian fluid, which returns to the parabolic profile at the end of the pulse. Fig. 9 presents the velocity profiles for *case 2* and *Re* 1.4–3.5. Comparing the distributions for the two fluids they are found to be quite different. Although both profiles are parabolic

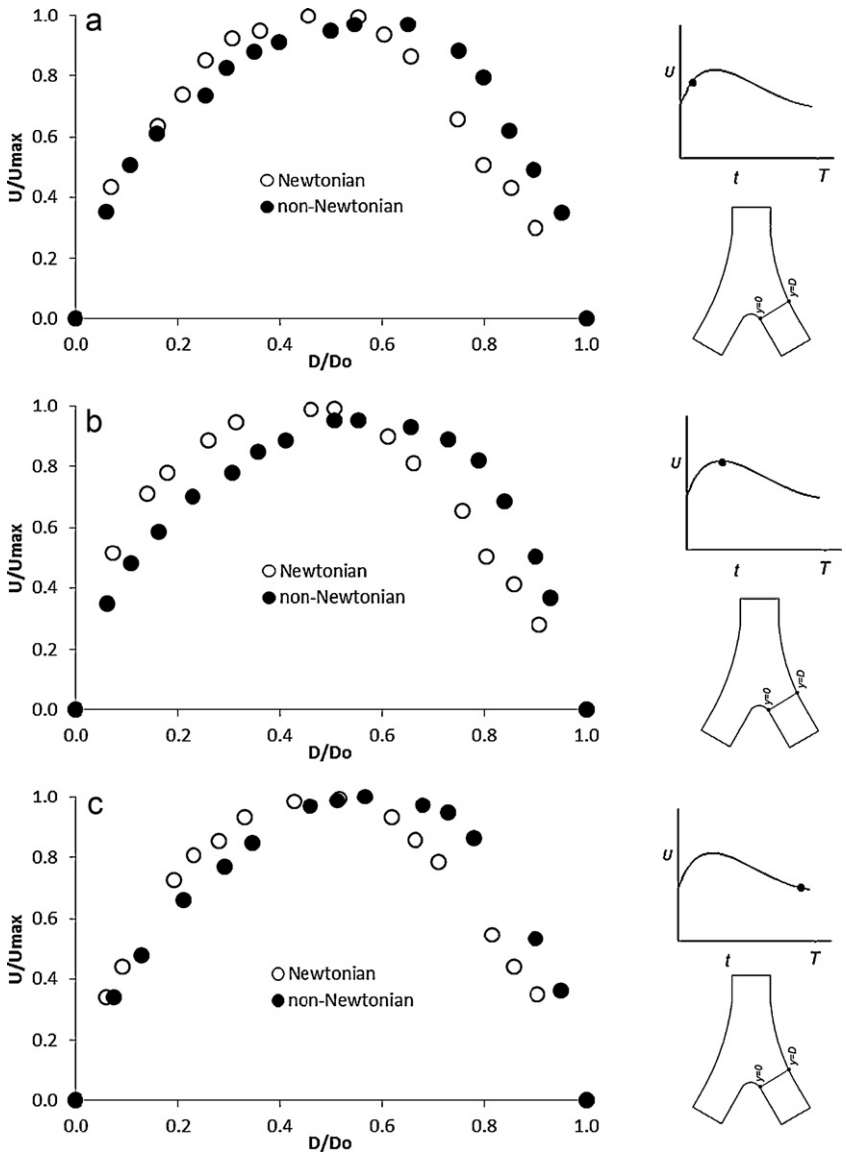

Fig. 9. Normalized velocity profiles with respect to their maximum value for Newtonian and non-Newtonian fluid at *station 2* for each instant of the pulse for *case 2* (*Re* = 1.4–3.5).

during a full pulse, the non-Newtonian fluid, as expected, exhibits a flat velocity profile.

The velocity data near the wall are utilized to estimate the *WSS*. Fig. 10 presents the *WSS*, normalized with respect to the maximum shear stress of the *Newtonian analogue* ($\tau_{wN\max}$), on the inner wall of the bifurcation for three instants of the pulse for both fluids and for *case 1*. The *WSS* is always *lower* for the non-Newtonian fluid while this difference ranges from 30 up to 40% depending on the instant of

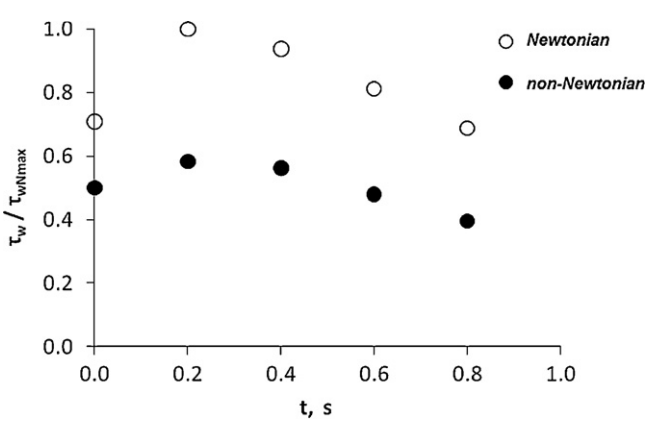

Fig. 10. Normalized wall shear stresses at the inner wall of the bifurcation during a pulse with respect to the maximum value (*case 1*).

Table 3
Comparison of the wall shear stress estimated for small arteries (present work) with data for large arteries (suprarenal and infrarenal aorta) obtained from [34].

Wall shear stress (Pa)	Peak	Minimum
Suprarenal aorta		
Anterior wall	4.80	−0.43
Posterior wall	5.40	−0.23
Infrarenal aorta		
Anterior wall	3.30	−0.69
Posterior wall	3.00	−0.75
Present work, case 1 (non-Newtonian)		
Outer wall	1.90	1.40
Inner wall	2.80	1.60
Present work, case 2 (non-Newtonian)		
Outer wall	0.65	0.45
Inner wall	0.70	0.50

Table 4
Comparison of the measured wall shear stress (*WSS*) for all stations.

WSS (Pa)	*Station 1*		*Station 2*		*Station 3*	
	Inner wall	Outer wall	Inner wall	Outer wall	Inner wall	Outer wall
Peak	2.37	2.37	2.80	1.9	2.18	2.18
Minimum	1.80	1.81	1.66	1.40	1.45	1.43

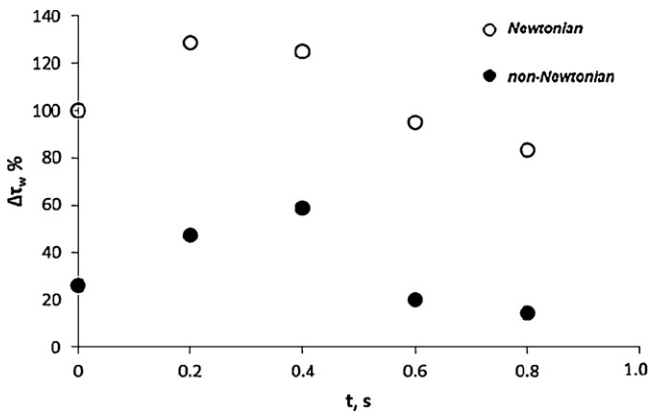

Fig. 11. Wall shear stress difference between the outer and the inner wall for the Newtonian and the non-Newtonian fluid [$\Delta\tau_w = (\tau_{w\ inner} - \tau_{w\ outer})/\tau_{w\ outer}$].

the pulse. This is because in *case 1* and for the Newtonian fluid the maximum of the axial velocity is shifted towards the inner wall. Consequently, higher velocities and shears rates occur. Generally the flow in bifurcated vessels is characterized by the skewing of velocity profile towards the inner wall. This is attributed to the lateral movement of fluid, i.e. from the outer towards the inner wall of the bifurcation, due to the pressure gradient developed and the centrifugal forces. As a result an area with relatively low *WSS* values is created along the outer walls [33].

Comparing the present results with those presented by Oshinski et al. [34], who conducted experiments *in vivo* for large arteries (Table 3), it is evident that *WSS* values in small arteries are quite different from those measured in large ones. In large vessels there are greater fluctuations of *WSS* during the whole pulse (−0.23 to 5.3 Pa on the posterior wall of the suprarenal aorta) compared with those in small vessels, where the range of shear stress was found to be between 1.6 and 2.8 Pa on the inner wall of the bifurcation (*station 2*). This is expected since in proximal arteries pulsatile flow is intense and attains even negative values (i.e. reversed velocity [10]). In Table 4 results of the estimated *WSS* for all the *stations* are presented. It must be noted that for *stations 1* and *2*, due to the symmetrical velocity profiles (Fig. 7b), there is no difference between the two walls, as expected.

Fig. 11 presents the % difference between the estimated *WSS* on the inner from that on the outer wall with respect to that of the outer wall, for both the Newtonian and the non-Newtonian fluid during a pulse. In both cases the stresses on the outer wall are lower which makes this area more predisposed to plaque formation.

7. Conclusions

The study of the blood rheology and of the dynamic characteristics of its flow is an important step towards comprehension, prediction, diagnosis and therapy of many cardiovascular diseases. The scope of this work was to study the pulsatile flow of a blood mimicking fluid in a *micro channel* that simulates a bifurcated small artery, in which the *Fahraeus–Lindqvist* effect is insignificant. The Reynolds numbers employed are relatively low, i.e. similar to those prevailing during blood flow in small arteries. Experiments using both a Newtonian and a non-Newtonian fluid (having asymptotic viscosity equal to the viscosity of the Newtonian one), proved that the common assumption that blood behaves as a Newtonian fluid is not valid for blood flow in small arteries. This is attributed to the shear thinning behavior of blood, which at the low shear rates encountered in small arteries results to a significant change of the velocity profile and consequently of the *WSS* and the hemodynamic forces. Thus by assuming that blood is a Newtonian fluid, the *WSS* is overestimated leading to an underestimation of the extent of the atherosclerosis-prone region. It was also proved that the outer wall of the bifurcation, as it is exposed to a *WSS* lower than the inner one, is more predisposed to atherosclerotic plaque formation.

Contrary to what it is known for large arteries, in small vessels, due to the fast decay of secondary flow (i.e. approximately one channel diameter downstream a bifurcation), low *WSS* values cover a rather limited area. It must be also added that, even though the *WSS* values estimated for small arteries are lower than those in the large ones, the difference between their extreme values is greater in large ones.

Generally the conclusions of this work could be extrapolated to every case with similar flow conditions (*Re* = 1–21) and diameters larger than 300 μm where *Fahraeus–Lindqvist* effect is insignificant. While this study did not directly assess atherosclerotic plaque formation, the results add the conjecture of evidence associating shear stress with atherosclerosis by focusing on small-sized arteries, i.e. a portion of the vasculature with important role in tissue perfusion. A direct, quantifiable dose–response investigation of flow-related parameters with the extent of atherosclerotic progression at the small arteries certainly merits further investigation in future work. Finally the experimental results of this project could be used for the validation of a computational fluid dynamic (*CFD*) code for further investigation of blood flow in small arteries.

Acknowledgments

The authors wish to acknowledge Asst. Professor A.A. Mouza and Dr. T. Goudoulas for their helpful comments and suggestions.

Conflict of interest statement

All authors state that there is no conflict of interest.

References

[1] Thiriet M. Biology and mechanics of blood flows part ii: mechanics and medical aspects. Paris: Springer; 2007.
[2] Chatzizisis YS, Giannoglou GD. Pulsatile flow: a critical modulator of the natural history of atherosclerosis. Med Hypotheses 2006;67:338–40.
[3] Shaaban AM, Duerinckx AJ. Wall shear stress and early atherosclerosis: a review. Am J Roentgenol 2000;174:1657–65.
[4] John LCH. Biomechanics of coronary artery and bypass graft disease: potential new approaches. Ann Thorac Surg 2009;87:331–8.
[5] Mouza AA, Pantzali MN, Paras SV, Tihon J. Experimental and numerical study of backward-facing step flow. In: 5th national chemical engineering conference. 2005.
[6] Chilian WM, Eastham CL, Marcus ML. Microvascular distribution of coronary resistance in beating left ventricle. Am J Physiol Heart Circ Physiol 1986;251:H779–88.
[7] Kuo L, Davis MJ, Cannon MS, Chilian WM. Pathophysiological consequences of atherosclerosis extend into the coronary microcirculation. Restoration of endothelium-dependent responses by L-arginine. Circ Res 1992;70:465–768.

[8] Bund SJ, Tweddel A, Hutton I, Heaquerty AM. Small artery structural alterations of patients with microvascular angina (syndrome X). Clin Sci (Lon) 1996;91:739–43.
[9] Aboyans V, Lacroix P, Criqui MH. Large and small vessels atherosclerosis: similarities and differences. Prog Cardiovasc Dis 2007;50:112–25.
[10] Truskey GA, Yuan F, Katz DF, editors. Transport phenomena in biological systems. NJ: Upper Saddle River; 2004.
[11] Artoli AM, Hoekstra AG, Sloot PMA. Mesoscopic simulations of systolic flow in the human abdominal aorta. J Biomech 2006;39:873–84.
[12] Giannoglou GD, Chatzizisis YS, Sianos G, Tsikaderis D, Matakos A, Koutkias V, et al. Integration of multi-modality imaging for accurate 3D reconstruction of human coronary arteries in vivo. Nucl Instrum Methods Phys Res A 2006;569:310–3.
[13] Gijsen FJH, Allanic E, Van De Vosse FN, Janssen JD. The influence of the non-Newtonian properties of blood on the flow in large arteries: unsteady flow in a 90 (curved tube). J Biomech 1999;32:705–13.
[14] Gijsen FJH, Van De Vosse FN, Janssen JD. The influence of the non-Newtonian properties of blood on the flow in large arteries: steady flow in a carotid bifurcation model. J Biomech 1999;32:601–8.
[15] Huo Y, Kassab GS. Pulsatile blood flow in the entire coronary arterial tree: theory and experiment. Am J Physiol Heart Circ Physiol 2006;291:H1074–87.
[16] Long Q, Xu XY, Ariff B, Thom SA, Hughes AD, Stanton AV. Reconstruction of blood flow patterns in a human carotid bifurcation: a combined CFD and MRI study. J Magn Reson Imaging 2000;11:299–311.
[17] Fujiwara H, Ishikawa T, Lima R, Matsuki N, Imai Y, Kaji H, et al. Red blood cell motions in high-hematocrit blood flowing through a stenosed micro channel. J Biomech 2009;42:838–43.
[18] Lima R, Wada S, Takeda M, Tsubota KI, Yamaguchi T. In vitro confocal micro-PIV measurements of blood flow in a square microchannel: the effect of the haematocrit on instantaneous velocity profiles. J Biomech 2007;40:2752–7.
[19] Sugii Y, Okuda R, Okamoto K, Madarame H. Velocity measurement of both red blood cells and plasma of in vitro blood flow using high-speed micro PIV technique. Meas Sci Technol 2005;16:1126–30.
[20] Lee JY, Ji HS, Lee SJ. Micro-PIV measurements of blood flow in extraembryonic blood vessels of chicken embryos. Physiol Meas 2007;28:1149–62.
[21] Vennemann P, Kiger KT, Lindken R, Groenendijk BCW, Stekelenburg-De Vos S, Ten Hagen TLM, et al. In vivo micro particle image velocimetry measurements of blood–plasma in the embryonic avian heart. J Biomech 2006;39:1191–200.
[22] Sugii Y, Nishio S, Okamoto K. In vivo PIV measurement of red blood cell velocity field in microvessels considering mesentery motion. Physiol Meas 2002;23:403–16.
[23] Pries AR, Secomb TW. Blood flow in microvascular networks. In: Tuman FR, Durán NW, Ley K, editors. Microcirculation. 2nd ed. San Diego: Academic Press; 2008.
[24] Fournier RL. Basic transport phenomena in biomedical engineering. New York: Taylor & Francis Group, LLC; 2007.
[25] Mabotuwana TD, Cheng LK, Pullan AJ. A model of blood flow in the mesenteric arterial system. BioMed Eng OnLine; 2007.
[26] Stamatopoulos C, Papaharilaou Y, Mathioulakis DS, Katsamouris A. Steady and unsteady flow within an axisymmetric tube dilatation. Exp Therm Fluid Sci 2010;34:915–27.
[27] Siouffi M, Pelissier R, Farahifar D, Rieu R. The effect of unsteadiness on the flow through stenoses and bifurcations. J Biomech 1984;17:299–315.
[28] Pantzali MN, Mouza AA, Paras SV. Counter-current gas–liquid flow and incipient flooding in inclined small diameter tubes. Chem Eng Sci 2008;63:3966–78.
[29] Lou Z, Yang W-J, Stein PD. Errors in the estimation of arterial wall shear rates that result from curve fitting of velocity profiles. J Biomech 1993;26:383–90.
[30] Cho YI, Kensey KR. Effects of the non-Newtonian viscosity of blood on flows in a diseased arterial vessel. 1. Steady flows. Biorheology 1991;28:241–62.
[31] Shin S, Keum DY. Measurement of blood viscosity using mass-detecting sensor. Biosens Bioelectron 2002;17:383–8.
[32] Paras SV. Secondary flow near bifurcations at low Reynolds numbers. MSc Thesis, University of Washington; 1979.
[33] Chen J, Lu XY. Numerical investigation of the non-Newtonian blood flow in a bifurcation model with a non-planar branch. J Biomech 2004;37:1899–911.
[34] Oshinski JN, Ku DN, Mukundan S, Loth F, Pettigrew RI. Determination of wall shear stress in the aorta with the use of MR phase velocity mapping. J Magn Reson Imaging 1995;5:640–7.